Vibration analysis of seedling picking mechanism based on EEMD-MA

Xin Jin[1,2], Shaofan Li[1], Mingyong Li[1*], Xiaowu Zhu[1], Guoqing Zhao[1], Mengnan Liu[3], Xiaolin Xie[1]

(1. *College of Agricultural Equipment Engineering, Henan University of Science and Technology, Luoyang 471003, Henan, China*;
2. *Science & Technology Innovation Center for Completed Set Equipment, Longmen Laboratory, Luoyang 471000, Henan, China*;
3. *First Tractor Company Limited, Luoyang 471003, Henan, China*)

Abstract: Aiming at the problems such as high substrate damage rate and low seedling picking success rate of the seedling picking mechanism of automatic vegetable transplanters under high-speed operation, this paper proposes an EEMD-MA method combining signal processing and modal analysis. Taking the cam-linked planetary gear system automatic seedling picking mechanism as the research object, this paper conducts research and analysis on its key component—the planet carrier. Sensitive components of vibration signals are extracted, and it is found that resonance is the critical factor deteriorating seedling picking performance. Subsequently, sequential quadratic programming is adopted to carry out optimal design of the component, and vibration tests as well as seedling picking tests are performed on the optimized seedling picking mechanism. The results show that the amplitude at the sensitive component decreased by 61.36%. At seedling picking speeds of 90, 100, 110, and 120 seedlings per minute, the average seedling picking success rate increased by 3.3%, 3.4%, 2.6%, and 1.8% respectively, while the average substrate damage rate decreased by 13.53%, 11.88%, 9.15%, and 8.12% respectively. The tests verify the effectiveness and practicability of the proposed method.

Keywords: ensemble empirical modal decomposition, planetary carrier, finite element analysis, vibration signal, seedling picking test

DOI: 10.25165/j.ijabe.20261904.10489

Citation: Jin X, Li S F, Li M Y, Zhu X W, Zhao G Q, Liu M N, et al. Vibration analysis of seedling picking mechanism based on EEMD-MA. Int J Agric & Biol Eng, 2026; 19(4): 112–122.

1 Introduction

Automatic vegetable transplanters overcome the limitations of manual seedling picking and feature advantages such as high operation efficiency and low labor intensity[1]. As the core component of automatic vegetable transplanters, the automatic seedling picking mechanism undertakes the most critical procedure in vegetable transplanting, and its efficient and stable seedling picking performance directly determines the overall transplanting quality[2-4]. However, during high-speed transplanting operations, the increased operating frequency of the automatic seedling picking mechanism induces vibration of its components. This leads to problems including damage to plug seedling substrates and seedling falling during seedling clamping, which further results in seedling picking failure, reduced seedling survival rate, and crop yield loss[5,6]. This severely restricts the working efficiency of automatic transplanters under high-speed operation and impairs transplanting quality, which will greatly hinder the popularization of such equipment. Therefore, research and vibration analysis on automatic seedling picking mechanisms under high-speed working conditions are of great significance for improving the quality and efficiency of transplanting operations.

In recent years, scholars at home and abroad have conducted extensive research on automatic seedling picking mechanisms[7,8]. Zhou et al.[9] designed an automatic seedling picking mechanism based on planetary Bézier gears and established its kinematic model. ADAMS software was used to construct and simulate the virtual model, and a physical prototype was manufactured. Physical tests showed that the seedling picking success rate reached 98.2% at a picking frequency of 150 r/min. The results of theoretical analysis, model simulation, and physical prototype tests are consistent, which verifies the practicability and effectiveness of the designed automatic seedling picking mechanism. Ye et al.[10] designed an automatic seedling picking mechanism composed of incomplete non-circular gears and planetary gear trains to address the problems of low transplanting efficiency and poor adaptability of transplanting machinery. They established a parameter correction model for optimal design and constructed an inverse design model, and the feasibility of the mechanism was verified through simulation analysis. Yin et al.[11] researched and designed a three-arm seedling picking mechanism, established its kinematic model, analyzed its motion trajectory, and validated the model via simulation software and theoretical analysis. Under the high-speed working condition of 180 seedlings per minute, the mechanism achieved a relatively high seedling picking success rate, yet substrate damage of plug seedlings still occurred. Liu et al.[12] obtained the optimal seedling picking trajectory based on human-computer interaction and designed a planetary non-circular gear mechanism. Trajectory simulation was carried out with simulation software, and idle running tests were conducted to verify the consistency among theoretical, simulated, and actual trajectories. Seedling picking experiments revealed that although the seedling picking success rate remained relatively high, the substrate damage rate and the number of damaged plug seedlings rose continuously as the seedling picking frequency increased. To solve the problem of low manual operation efficiency of semi-automatic transplanters, Hu et al.[13] designed a

Received date: 2026-02-06 **Accepted date:** 2026-06-26

Biographies: Xin Jin, PhD, Professor, research interest: vegetables intelligent production and agricultural sensors, Email: jx.771@163.com; **Shaofan Li**, MS candidate, research interest: agricultural engineering, Email: 2559572249@qq.com; **Xiaowu Zhu**, PhD Scholar, research interest: agricultural engineering and information technology, Email: zhuxiaowu620@163.com; **Guoqing Zhao**, MS candidate, research interest: agricultural engineering, Email: 3165399625@qq.com; **Mengnan Liu**, Researcher, research interest: drivetrain and intelligent control technology for tractors, Email: liumengnan27@163.com; Xiaolin Xie, PhD, Associate Professor, research interest: agricultural intelligent power equipment, Email: xiexiaolin@haust.edu.cn.

***Corresponding author: Mingyong Li**, PhD, Associate Professor, research interest: agricultural information and intelligent machine. College of Agricultural Equipment Engineering, Henan University of Science and Technology, Luoyang 471003, China. Tel: +86-379-64877817, Email: mingyonglee@163.com.

stem-clamping automatic seedling picking mechanism. A novel seedling picking trajectory was developed based on the double crank-linkage mechanism, and the feasibility of the mechanism was verified. Meanwhile, seedling picking tests were carried out at different frequencies. The results indicated that the increase of picking frequency would reduce the seedling picking success rate, and the vibration generated by the mechanism under high picking frequencies would impair transplanting quality. It can be seen from the above literature review that as the seedling picking frequency rises, vibration occurs on seedling picking components of automatic seedling picking mechanisms, resulting in a lower seedling picking success rate and higher substrate damage rate of plug seedlings. Although numerous scholars have observed this phenomenon, they only carried out structural optimization design without conducting in-depth research and analysis on the root causes of vibration.

Studies on vibration phenomena are generally conducted from two perspectives: vibration signal analysis and modal analysis. Vibration signal analysis mainly acquires vibration signals of the mechanism through signal receiving devices such as sensors, and processes the vibration signals with a series of analytical methods to extract characteristic vibration information of the signals. Su et al.[14] studied the influence of transplanter vibration on planting quality, derived a mathematical model describing vibration characteristics of the transplanter-soil system, and carried out vibration tests. The test results indicated that vertical vibration was the most intense, with its frequency ranging from 4.5 to 5.5 Hz and increasing along with the operating speed. Chowdhury et al.[15] investigated the vibration issues of vegetable transplanters and conducted vibration tests under transplanting operations at different travel speeds and loads. Power spectral density (PSD) analysis was adopted to identify the dominant vibration frequencies. The test results demonstrated that the daily vibration exposure value A(8) and vibration dose value (VDV) varied in the ranges of 10-15 m/s^2 and 20-31 $m/s^{1.75}$, respectively, both exceeding the limits specified in ISO 2631-1 standard. Zhu et al.[16] analyzed the influence of vibration of the seedling feeding device on transplanting operations, optimized the device based on vibration analysis, and carried out corresponding tests. The test results show that under the optimal parameter combination, the vibration of the transplanter is effectively alleviated and the operation performance reaches the optimum. Modal analysis mainly focuses on investigating structural characteristics such as natural frequencies and mode shapes of each order: Jin et al.[17] analyzed the vibration problems of high-speed rice transplanters under normal operating conditions by means of modal tests and finite element modal analysis. The research results provide references for subsequent vibration reduction optimization design. Chen et al.[18] addressed the severe vibration and structural deformation of rice combine harvesters during field operations. They carried out modal analysis and vibration response tests on the frame, which verified the validity of the dynamic model. Meanwhile, it was found that the sixth-order natural frequency fell within the resonance frequency range, offering reference significance for further optimization and improvement of the frame. An in-depth exploration of the influence of mechanical vibration on high-speed transplanting operations is essential for structural optimization, vibration suppression, and efficiency improvement of seedling picking mechanisms. Therefore, it is urgent to carry out targeted research on the vibration problems of automatic seedling picking mechanisms under high-speed working conditions.

To address the degradation of transplanting quality and operational efficiency caused by decreased seedling picking success rate and increased substrate damage rate due to vibration of automatic seedling picking mechanisms under high-speed working conditions, this paper conducts an in-depth analysis on the cam-linked planetary gear system automatic seedling picking mechanism designed by the research group, as shown in Figure 1. The main

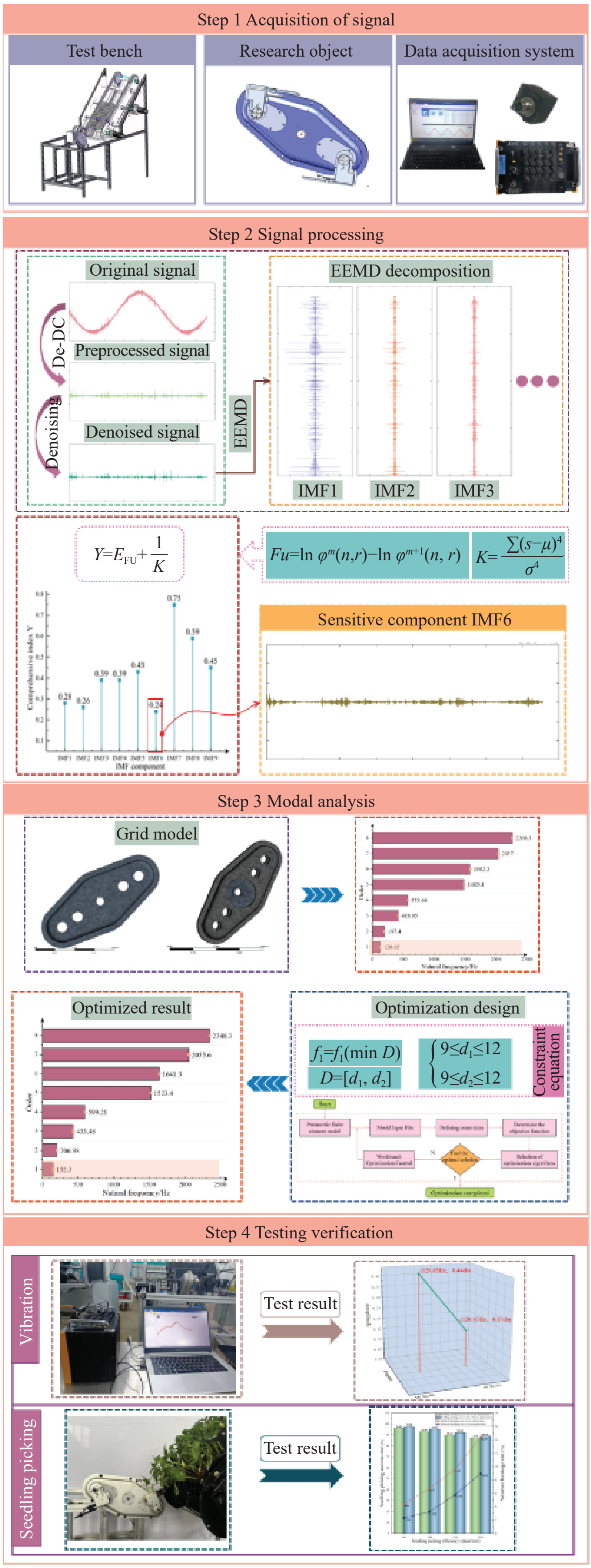

Figure 1 Research flowchart of seedling picking mechanism based on EEMD-MA

research contents are as follows: (1) A notch filter was designed for signal preprocessing, and a method combining ensemble empirical mode decomposition (EEMD) and finite element modal analysis (EEMD-MA) was proposed. (2) A comprehensive index Y was constructed to select sensitive components of signals and extract their characteristic frequencies. (3) NLPQL algorithm was adopted to optimize the planet carrier, so as to adjust its inherent characteristics and avoid resonance. This research can promote the improvement of transplanting quality, reduce the substrate damage rate of plug seedlings, and is of great significance for the optimal design of high-speed transplanting equipment.

2 Materials and methods

2.1 Composition and working principle of the automatic vegetable transplanter

The test bench for the automatic vegetable transplanter was designed by our research group[19], as shown in Figure 2a. The transplanter consists of the seedling feeding mechanism, the seedling picking mechanism, and the overall machine control system, with motors adopted as driving devices. Among them, the cam-linked planetary gear system automatic seedling picking mechanism is composed of three parts: the cam-linkage mechanism, planetary gear train, and seedling picking arm, as shown in Figure 2b.

Figure 3 illustrates the structural composition of the cam-linked planetary gear system automatic seedling picking mechanism. Within this mechanism, the input shaft driving the cam-linkage assembly and the planet carrier that drives the planetary gear train are two critical components in power transmission.

Specifically, the cam drives the driven rod to move via the linkage structure, while rotation of the planet carrier enables meshing between the planetary gears mounted on it, which in turn generates counter-rotational motion relative to the carrier. During the seedling picking operation of the mechanism, the motor drives the input shaft to rotate, and power is transmitted to the cam through the input shaft. The rotation of the cam pushes the roller to move along the cam profile. Meanwhile, the sun gear rotates under the combined action of the cam and connecting rods. Power is transmitted to the planet carrier via the cam-linkage mechanism, and the rotation of the planet carrier drives the planetary gear train to operate. Meanwhile, power is delivered to the seedling picking arm through the output shaft to realize clamping and releasing of plug seedlings.

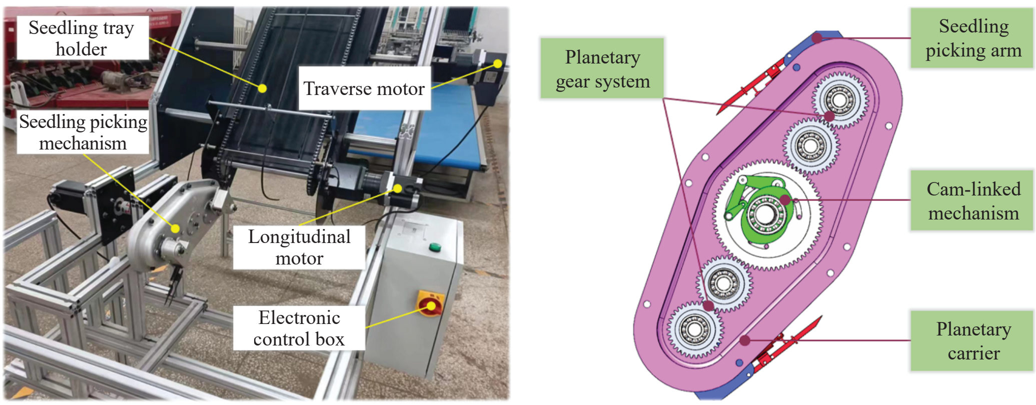

a. The automatic vegetable transplanting machine test bench

b. The cam-linked planetary gear system automatic seedling picking mechanism

Figure 2 Schematic diagram of the whole vegetable transplanter and its automatic seedling picking mechanism

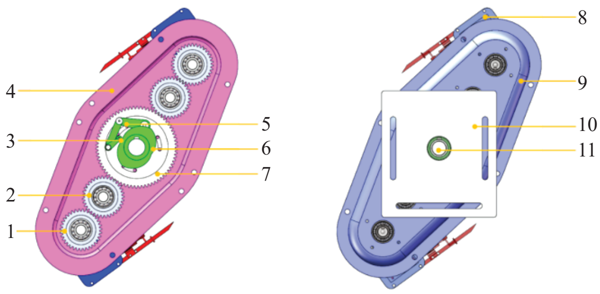

1. Planetary gear; 2. Intermediate gear; 3. Roller; 4. Left shell; 5. Linkage mechanism; 6. Cam; 7. Sun gear; 8. Seedling picking arm; 9. Right shell; 10. Rack mounting plate; 11. Input shaft.

Figure 3 Structural composition of the automatic seedling picking mechanism

During high-speed operation of the cam-linked planetary gear system automatic seedling picking mechanism, vibration of its key component, the planet carrier, will exert adverse effects on seedling picking performance, as presented in Figure 4: (1) Positioning deviation occurs between seedling picking needles and plug tray holes, resulting in damage to plug seedlings. (2) Vibration of the mechanical structure when seedling picking needles are inserted into the plug tray causes severe damage to the substrate and increases the substrate damage rate. (3) Vibration causes jitter of seedling picking needles during the seedling holding stage, leading to unstable seedling clamping and seedling falling off. In summary, research on the vibration of the planet carrier in the seedling picking mechanism possesses extremely important value and significance.

2.2 Test equipment and methods

2.2.1 Test equipment

The test object is the planet carrier of the seedling picking mechanism. The main required equipment includes three-axis acceleration sensors, DH5902 dynamic signal acquisition instrument, computer, and the test bench of the automatic vegetable transplanter. Among them, the three-axis acceleration sensor is Model 356A16 manufactured by PCB, USA; the DH5902 dynamic signal acquisition instrument is produced by Donghua Testing Technology Co., Ltd. The specific parameters of the above equipment are listed in Table 1.

2.2.2 Test method

In this test, vibration signals are obtained through direct measurement during the operation of the seedling picking mechanism, which can effectively analyze its vibration characteristics under working conditions. This method features high authenticity, simple operation, and convenient testing.

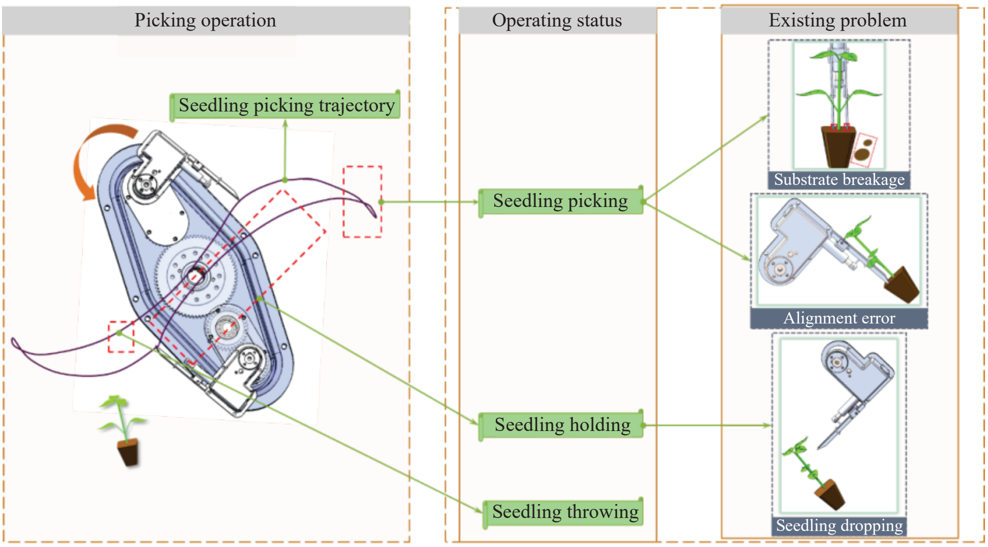

Figure 4 Schematic diagram of the influence of planetary carrier vibration

Table 1 Vibration test equipment information

Equipment	Type	Parameter	Value	Manufacturer
Dynamic signal acquisition instrument	DH5902	Number of channels	16	Donghua Testing Technology Co., Ltd.
		Maximum sampling frequency/kHz	100	
		Signal input method	IEPE	
Laptop	Aspire A315	Processor	Intel(R) Core (TM) i7-10510	Acer Incorporated
Three-axis acceleration sensor	356A16	Frequency response range: kHz	0.3-6.0	PCB Piezotronics, Inc. of the United States
		Sensitivity: mV/g	100 (±10%)	
		Measurement range: m/s² pk	±50	

The detailed test procedure is illustrated in Figure 5. Firstly, the three-axis acceleration sensor is fixed at the designated position of the planet carrier. Considering the symmetrical structure of the planet carrier and to avoid interference from the seedling picking arm during operation, the sensor is mounted above the central symmetry line on the non-fixed connecting surface of the planet carrier. Connect the sensor, data acquisition analyzer, laptop, and other test equipment in sequence with connecting wires. After all connections are checked and confirmed correct, start the test bench, and the seedling picking mechanism begins the seedling picking operation. During operation, the planet carrier performs periodic rotation around the input shaft and generates forced vibration simultaneously. The vibration signals are transmitted from the sensor to the signal acquisition instrument, then stored in the laptop via dynamic signal acquisition and analysis software.

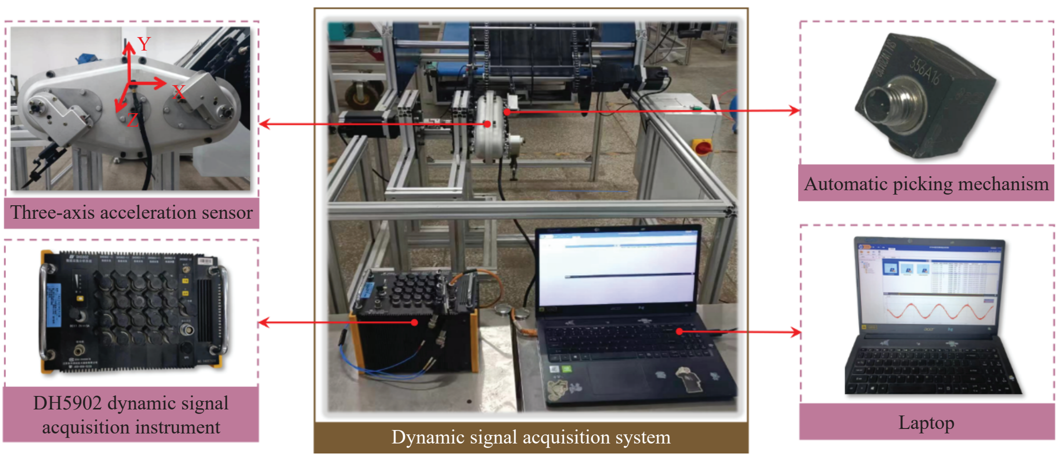

Figure 5 Vibration test and test equipment

Since the planet carrier rotates, the sensor will rotate along with it, which will twist the connecting wires. In severe cases, the wires may separate from the sensor and fall off, leading to failure of the vibration test. To prevent this problem, the following points should be noted during the test: (1) Signal collection shall be carried out only after the seedling picking mechanism runs stably. At the initial stage of collection, large vibration will be generated by motor startup and the initial rotation of the mechanism, and the collected signals will contain random impact components, which will seriously interfere with subsequent analysis. (2) The sensor and acquisition analyzer are connected via a sensor connector, and the measured position rotates during operation. During signal acquisition, avoid collision and contact between the sensor connector and seedling picking claws, otherwise signal collection will be disturbed.

2.3 Vibration analysis

2.3.1 Ensemble empirical mode decomposition

Proposed by Huang et al. in 1998, Empirical Mode

Decomposition (EMD) is an algorithm for processing and analyzing nonlinear and non-stationary random signals. EMD can adaptively decompose the original nonlinear signal into several Intrinsic Mode Functions (IMFs) and a residual component according to different time scales. It has been widely applied in signal analysis, speech recognition, and other fields[20-22]. However, EMD itself has many drawbacks, such as high sensitivity to noise and mode mixing[23-25].

Ensemble Empirical Mode Decomposition (EEMD) is an improved algorithm based on Empirical Mode Decomposition (EMD). It decomposes signals after adding Gaussian white noise to the original signal[26]. In the EEMD method, the added white noise features a uniformly distributed frequency spectrum and a zero mean value. Therefore, the introduction of white noise can adjust the extremum characteristics of the signal, so as to effectively alleviate the end effect and mode mixing existing in EMD[27]. Specific implementation steps of EEMD:

(1) Different white noise sequences $\omega_i(t)$ are added to the original signal $X(t)$ to obtain multiple groups of new noisy signals $X'(t)$:

$$X'(t) = X(t) + \omega_i(t) \tag{1}$$

(2) EMD decomposition is carried out on each new signal with added noise, and each group obtains its own multi-order IMF components and residual component RES:

$$X'(t) = \sum_{i=1}^{m} \mathrm{IMF}_i + \mathrm{RES} \tag{2}$$

(3) The obtained IMF components of the same order from all groups are averaged integrally, and a set of final IMF components $I_j(t)$ can be acquired:

$$I_j(t) = \frac{1}{M}\sum_{i=1}^{M} I_{i,j}(t),\quad 1 \le j \le m+1 \tag{3}$$

where, $I_{i,j}(t)$ is the j-th IMF component decomposed after adding white noise for the i-th time; $I_j(t)$ is the final j-th IMF component.

2.3.2 Kurtosis and fuzzy entropy

Fuzzy Entropy is an improved algorithm derived from sample entropy. The fuzzy set theory was proposed by Zadeh[28] in 1968. This method uses the mean value of signals instead of absolute amplitude difference, and adopts the exponential function as the fuzzy function to measure the consistency between two vectors. In signal analysis, the measured signal is taken as the sample set to calculate its fuzzy entropy. A larger value indicates worse consistency of the signal; on the contrary, the consistency is better[29].

Kurtosis is a numerical statistic reflecting the distribution characteristics of random variables and a dimensionless indicator that is sensitive to impact components in signals[30]. The larger the kurtosis value, the richer the impact signals and characteristic information contained in the signal. During normal mechanical operation, the kurtosis value is approximately 3; under the effect of impact signals, the kurtosis value will be much greater than 3, making impact features easier to extract[31]. The definition formula of kurtosis is as follows:

$$K = \frac{\sum (s-\mu)^4}{\sigma^4} \tag{4}$$

where, s represents the vibration signal; μ is the mean value of vibration signal s; and σ denotes the standard deviation of the signal.

2.3.3 Signal analysis process

Signal analysis based on EEMD is often used for signal modal decomposition. However, relying solely on this method sometimes fails to accurately obtain the required characteristic information.

According to relevant literature, fuzzy entropy and kurtosis are combined to construct a comprehensive indicator for extracting signal characteristic information[32]. The definition of the comprehensive indicator Y is shown as follows:

$$Y = E_{\mathrm{FU}} + \frac{1}{K} \tag{5}$$

The comprehensive indicator Y can screen out the components containing the richest impact and characteristic information. Afterwards, envelope spectrum analysis is carried out on the obtained components to identify characteristic frequencies. After collecting the vibration signals of the planet carrier, preprocessing is required. Since the sensor performs periodic rotational movement together with the planet carrier, the collected signals contain DC components, so the vibration signals need to be preprocessed to eliminate DC components first. The processed signals are then handled as follows: (1) The preprocessed signals are denoised by wavelet soft thresholding, and EEMD adaptive modal decomposition is adopted after denoising to obtain the intrinsic mode components of the signals. (2) Calculate the comprehensive index Y of each component, select the component with the minimum comprehensive index as the sensitive component, and carry out subsequent feature extraction. (3) Analyze the screened intrinsic mode components and obtain their envelope spectra to acquire vibration characteristics.

3 Results and discussion

3.1 Vibration signal preprocessing

The time-domain diagrams of the original vibration signal and preprocessed signal are shown in Figure 6. Figure 6 illustrates that the seedling picking mechanism picks and drops seedlings twice within one rotation cycle, and a single seedling picking cycle is divided into three stages: seedling picking, seedling holding, and idling. The seedling dropping moment occurs at the end of the seedling holding stage and before the start of the idling stage, which is marked with an asterisk in the figure. It can also be clearly observed from Figure 6 that the signal presents a sinusoidal waveform. This is because the sensor is not arranged at the rotation center of the planet carrier and rotates periodically around the rotation center together with the planet carrier. In signal analysis, the DC component contained in the signal needs to be removed first to avoid interference with subsequent analysis. In addition, as an external excitation source, the motor also affects the vibration of the planet carrier, and the motor frequency and its frequency multiples should also be processed during signal preprocessing.

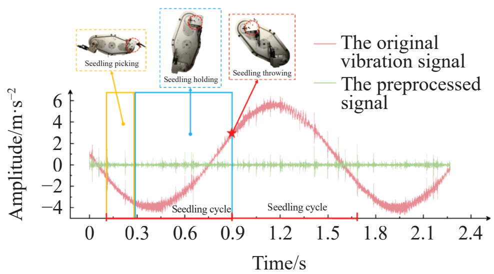

Note: The sinusoidal curve is generated by the periodic rotation of the sensor.

Figure 6 Time domain diagrams of original vibration signal and preprocessed signal

Figure 7 shows the frequency-domain diagrams of the original vibration signal and preprocessed signal. It can be seen from Figure 7 that the original vibration signal has the maximum peak value at zero frequency, which indicates an obvious DC component existing in the signal. The DC component in the signal will seriously interfere with subsequent signal decomposition and analysis. Therefore, a notch filter is adopted in this paper to eliminate the DC component for signal preprocessing. The waveform trend of the time-domain diagram of the preprocessed signal in Figure 6 is a straight line rather than a sinusoidal waveform, which indicates that the DC component in the original vibration signal has been effectively removed. It can also be seen from the frequency spectrum of the preprocessed signal in Figure 7 that the DC component has been eliminated. However, it can also be seen from the spectrogram that the preprocessed signal contains a large amount of noise interference, which is unfavorable to the subsequent analysis of signal features. Therefore, further denoising processing is required to facilitate the extraction of subsequent signal characteristic information.

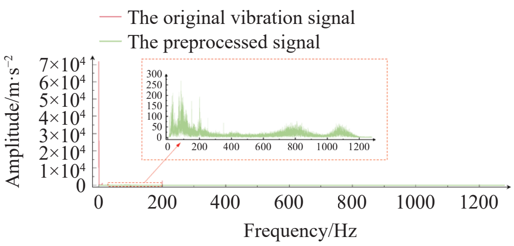

Figure 7 Frequency domain diagrams of original vibration signal and preprocessed signal

3.2 Signal analysis

The wavelet soft threshold method is used to denoise the preprocessed signal, and the results are shown in Figure 8 below. Compared with the preprocessed signal in Figure 6, the noise is greatly suppressed, which facilitates the subsequent research and analysis of the signal. In this study, the selected wavelet function is “db4” with a threshold of 0.1.

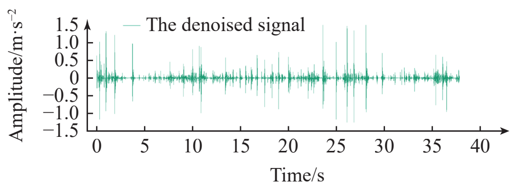

Figure 8 Time-domain diagram after denoising

The denoised signal is decomposed by the EEMD method. When selecting the number of modes a, preliminary pre-decompositions are carried out with a set to 7, 9, and 12 based on the analysis of vibration signals. Taking over-decomposition and modal aliasing into consideration, a is finally determined as 9. The decomposition results are shown in Figure 9. After EEMD decomposition, the signal is decomposed into eight IMF components and one residual term (RES) in descending order of frequency.

To obtain the sensitive components of the vibration signal, the fuzzy entropy and kurtosis of each IMF component are calculated respectively, and the comprehensive index Y is obtained as listed in Table 2.

It can be analyzed from Table 2 that among all components of the denoised vibration signal, the IMF6 component has the minimum comprehensive index Y, which is judged to possess the optimal sensitivity to the original signal. Analysis relying merely on vibration signals is relatively one-sided and cannot reflect the inherent characteristics of components. To further analyze the vibration characteristics of the planet carrier, in-depth research combined with the finite element model will be carried out subsequently.

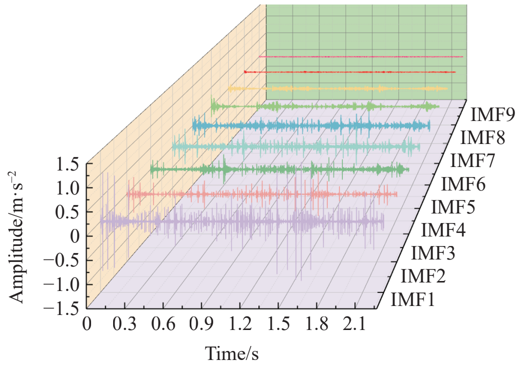

Figure 9 IMF components obtained by EEMD

Table 2 Calculation of characteristic quantities of each IMF component

IMFs	Kurtosis K	Fuzzy entropy FU	Comprehensive index Y
1	91.01	0.27	0.28
2	77.21	0.25	0.26
3	11.19	0.3	0.39
4	12.75	0.31	0.39
5	5.84	0.26	0.43
6	7.15	0.1	0.24
7	1.42	0.05	0.75
8	1.71	0.01	0.59
9	2.37	0.03	0.45

3.3 Structural optimization of planet carrier

The planet carrier has a length of 430 mm, a width of 240 mm, and a shell thickness of 10 mm. It is mainly made of ZL104A aluminum alloy through casting, sand removal, and aging treatment. Firstly, the three-dimensional modeling software SolidWorks is used to establish a virtual model of the planet carrier, and the model is imported into Ansys Workbench via plug-ins to obtain its finite element model. A more complex finite element model requires a larger amount of computation, so the model needs to be simplified on the premise of ensuring calculation accuracy. The simplification of the finite element model of the planet carrier is as follows: (1) Ignore minor details such as small holes and tiny chamfers on the part that have little influence on the overall structure; (2) Replace bolt connections linking the two shells with node coupling. After modeling is completed, mesh division is performed on the planet carrier. The material of the model is defined as aluminum alloy with a Poisson’s ratio of 0.33, elastic modulus of 7.1×10^{10} N/m^2, and mass density of 2.77×10^3 kg/m^3.

Then the model is simplified and constrained to make it closer to the actual working conditions. The constraint positions are the rotation center of the planet carrier and the plane adjacent to the frame fixing plate. Since the vibration generated by the planet carrier during operation hardly reaches high-order modes under normal circumstances, low-order modes exert a dominant influence on it. Therefore, only the first eight natural frequencies of the planet carrier are analyzed, as listed in Table 3.

When the seedling picking mechanism operates normally with an operating frequency of 90-120 seedlings per minute, the calculated excitation frequency ranges from 90.23 to 130 Hz. It can be seen from Table 3 that the first-order natural frequency of the planet carrier is 128.65 Hz, which falls exactly within this range. Therefore, during high-speed seedling picking operation of the mechanism, the excitation source will cause resonance of the planet carrier, thereby impairing the quality of transplanting operations. To avoid resonance, optimal structural design of the planet carrier shell is required to adjust its natural frequencies, especially the first-order natural frequency.

Table 3 Modal analysis results

Order	Modal frequency/Hz	Order	Modal frequency/Hz
1	128.65	5	1485.4
2	197.4	6	1582.2
3	418.85	7	2037.0
4	573.68	8	2260.3

Combined with the above finite element analysis results, the first-order natural frequency of the planet carrier under high-speed working conditions is taken as the optimization objective, and the structural redesign of the seedling picking mechanism's planet carrier is carried out to avoid resonance. During the optimization design, the constraint condition is set to minimize the increase of wall thickness so as to prevent sharp growth of the overall mass.

According to practical conditions, the Direct optimization module in ANSYS is selected for parameter configuration. The mathematical model and constraint conditions for the structural optimization of the planet carrier are given as follows:

$$f_1 = f_1(\min D) \tag{6}$$

$$D = [d_1,\ d_2] \tag{7}$$

$$\begin{cases} 9 \le d_1 \le 12 \\ 9 \le d_2 \le 12 \end{cases} \tag{8}$$

where, f_1 denotes the first-order natural frequency of the planet carrier; d_1 stands for the thickness of the left shell of the planet carrier, mm; d_2 represents the thickness of the right shell of the planet carrier, mm.

Adjusting the shell thickness brings low manufacturing cost, has no interference with the installation of gears, input and output shafts, and other components inside the seedling picking mechanism, and keeps the seedling picking trajectory unchanged. Therefore, shell thicknesses are selected as design variables to adjust the natural modal frequencies of the planet carrier. After finishing parameter configuration, the NLPQL algorithm is adopted according to the selected design variables and objective function. The flow chart of optimization is shown in Figure 10 below.

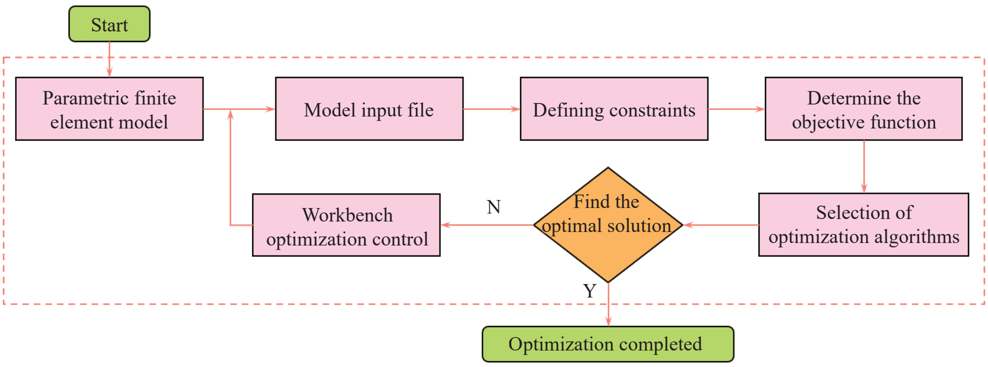

Figure 10 Optimization design flow chart

Under the premise of adjusting the first-order natural frequency of the planet carrier, minimizing mass increment, and keeping away from the excitation frequency range as far as possible, the optimized thicknesses of the left and right shells of the planet carrier are 9.7 mm and 11.5 mm respectively. The first eight natural frequencies of the optimized planet carrier are listed in Table 4. The first-order natural frequency reaches 152.3 Hz, and the other seven orders are 206.98 Hz, 433.98 Hz, 599.21 Hz, 1523.4 Hz, 1641.3 Hz, 2055.6 Hz, and 2348.3 Hz, all of which are outside the excitation frequency band.

Table 4 Modal analysis results of optimized planet carrier

Order	Modal frequency/Hz	Order	Modal frequency/Hz
1	152.3	5	1523.4
2	206.98	6	1641.3
3	433.48	7	2055.6
4	599.21	8	2348.3

3.4 Modal analysis results of optimized planet carrier

After processing and assembly, the optimized structure was tested for performance in the Agricultural Machinery Operation Laboratory of Henan University of Science and Technology. The field tests mainly consist of vibration test and seedling picking test. The vibration test aims to analyze whether the vibration of sensitive components of the optimized planet carrier is reduced during normal operation from the vibration perspective. The seedling picking test directly tests the influence of the optimized planet carrier on the operation quality of the seedling picking mechanism, and compares the seedling picking performance before and after optimization.

3.4.1 Vibration test

The test methods and equipment adopted in the vibration test are consistent with those described in Section 2.2.1. The sensor layout positions and the rotation frequency of the planet carrier during the test are identical to those used in the vibration test before optimization. After collecting vibration signals in the test, EEMD decomposition is performed on the signals, and envelope spectrum analysis is carried out for sensitive components.

It can be seen from Figure 11 that before the structural optimization of the planet carrier, the maximum vibration intensity reaches 0.44 dB at the frequency of 129.83 Hz. In addition, combined with the analysis of the excitation source in Section 3.1, this frequency is selected as the main characteristic frequency for the analysis after eliminating frequency points near the excitation source. It can be concluded from Figure 12 that the vibration intensity of the optimized planet carrier at the characteristic frequency is 0.17 dB, which is reduced by 61.36% compared with that before optimization, verifying that the optimized planet carrier can effectively suppress vibration intensity.

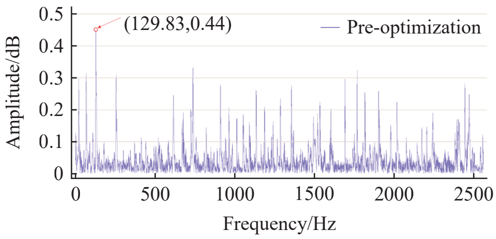

Figure 11 Envelope spectrum of sensitive component IMF6 before optimization

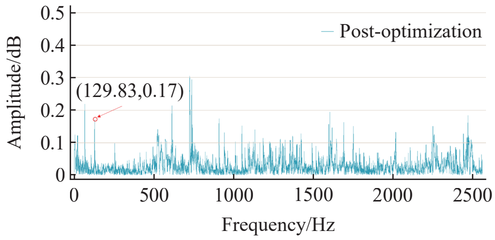

Figure 12 Envelope spectrum of sensitive component IMF6 after optimization

3.4.2 Seedling picking test

According to the requirements specified in Dry Land Transplanting Machinery, the operating efficiency of high-speed transplanters shall be higher than 90 seedlings per minute. During the test, the seedling picking frequencies were set to 90 seedlings/min, 100 seedlings/min, 110 seedlings/min, and 120 seedlings/min respectively. Three groups of tests were carried out under each seedling picking frequency, with a sample size of 128 pepper seedlings in each group. A 16×8 plug tray and pepper seedlings cultivated at Suzhou Limin Seedling Breeding Base were adopted to verify the seedling picking performance of the optimized seedling picking mechanism. The physical properties of the pot seedlings are as follows: substrate moisture content 60%, seedling age 30 d, seedling height 10-15 cm. An electronic balance with an accuracy of 0.1 g was used to measure the substrate weight of each pot seedling before the seedling picking test, and the average mass of pot seedlings was calculated. The seedling picking success rate C_1 and substrate damage rate C_2 were taken as evaluation indicators, and the calculation formulas are given as follows:

$$C_1 = \frac{q}{Q} \times 100\% \tag{9}$$

$$C_2 = \left(1 - \frac{m}{M}\right) \times 100\% \tag{10}$$

where, Q represents the total number of pot seedlings in the test; q denotes the total number of pot seedlings successfully picked and released at the seedling dropping position; M is the average substrate mass before seedling picking; m stands for the average substrate mass after successful seedling picking.

Figure 13 shows the seedling picking operation diagram of the optimized planet carrier. Table 5 presents the statistical data of seedling picking tests before and after optimization. It can be seen from Table 5 and Figure 14 that the optimized seedling picking mechanism achieves remarkable improvements in increasing seedling picking success rate and reducing substrate damage rate, which also indicates that the planet carrier plays a vital role in the cam-linked planetary gear system automatic seedling picking mechanism. It is obvious from Figure 14 that the substrate damage rate rises and the seedling picking success rate declines with the increase of seedling picking frequency. Compared with the original mechanism before optimization, the optimized one achieves an obvious reduction in substrate damage rate under the high-speed operation of 120 seedlings per minute. This proves that the optimized seedling picking mechanism can greatly cut down substrate damage and improve the operation quality of the transplanter.

Figure 13 Seedling picking test

Table 5 Statistical table of test results before and after optimization

Group	Seedling picking efficiency/plant·min^{-1}	Number of successful seedling picking/plant		Seedling picking success rate/%		Substrate breakage rate/%		Average seedling picking success rate/%		Average substrate breakage rate/%	
		a	b	a	b	a	b	a	b	a	b
1		120	125	93.75	97.65	4.52	3.89				
2	90	123	124	96.09	96.87	4.50	3.91	94.53	97.65	4.51	3.9
3		120	126	93.75	98.43	4.52	3.91				
1		115	120	89.84	93.75	6.25	5.48				
2	100	118	122	92.19	95.31	6.24	5.48	91.41	94.53	6.23	5.49
3		118	121	92.19	94.53	6.21	5.5				
1		115	119	89.84	92.96	9.85	8.94				
2	110	116	117	90.62	91.4	9.86	8.96	89.84	92.18	9.84	8.94
3		114	118	89.06	92.18	9.82	8.91				
1		110	112	85.94	87.5	14.28	13.1				
2	120	113	115	88.28	89.84	14.3	13.15	86.72	88.28	14.28	13.12
3		110	112	85.94	87.5	14.27	13.1				

Note: a—Test results before optimization; b—Test results after optimization.

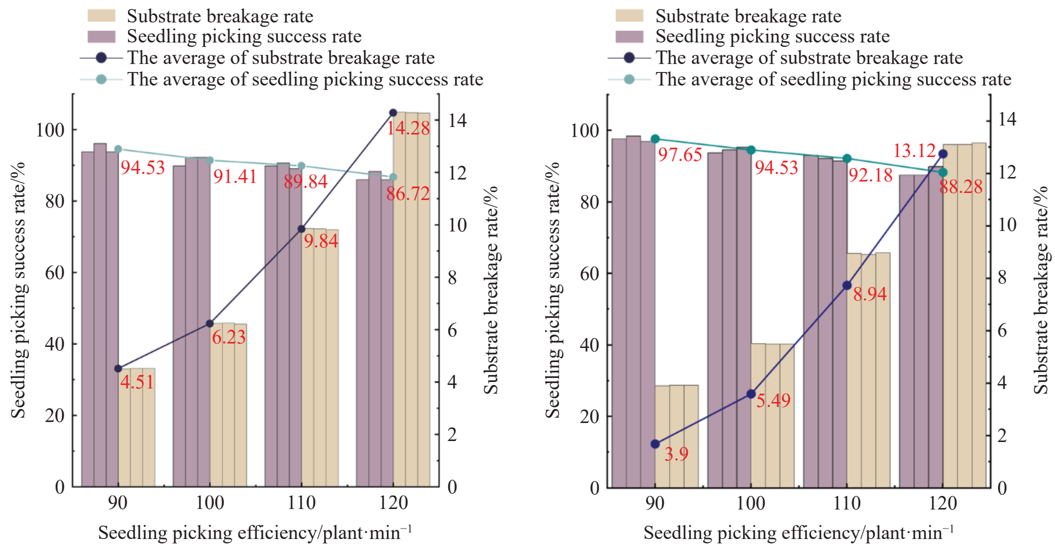

a. Experimental results pre-optimization

b. Experimental results post-optimization

Figure 14 Statistical chart of test results before and after optimization

To clearly demonstrate the seedling picking test results before and after optimization, Figure 14 adopts bar charts and line charts to visually display the average seedling picking success rate and average substrate damage rate under different seedling picking frequencies.

Figure 15 illustrates the comparison of seedling picking test results before and after optimization. Figure 15a shows that under the same operating speed, the average seedling picking success rate of the optimized mechanism is improved to a certain extent compared with the original one, yet the success rate is still less than 90% under high-speed working conditions. Figure 15b reflects the variation of average substrate damage rate with seedling picking speed before and after optimization. The results reveal that at seedling picking frequencies of 90 seedlings/min, 100 seedlings/min, 110 seedlings/min, and 120 seedlings/min, the average substrate damage rate is reduced by 13.53%, 11.88%, 9.15%, and 8.12% respectively. In summary, the optimized seedling picking mechanism can effectively reduce the damage rate of pot seedling substrate while maintaining a favorable seedling picking success rate.

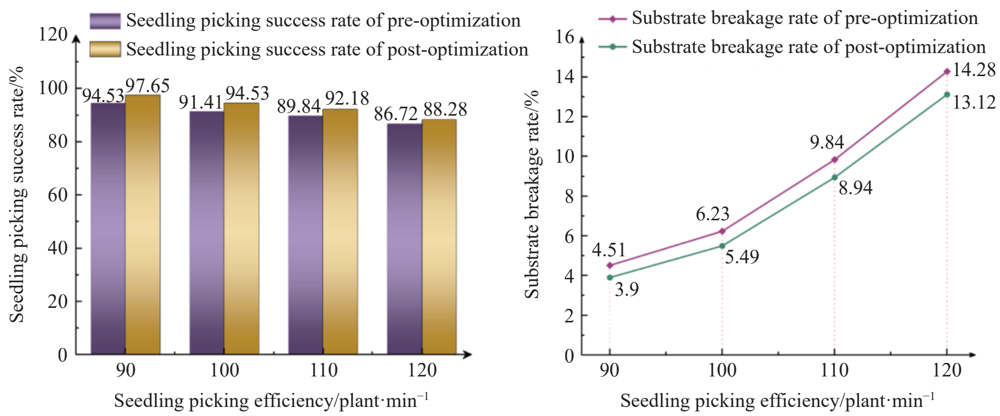

a. Seedling picking success rate

b. Substrate breakage rate

Figure 15 Comparison of seedling picking test results before and after optimization

Nevertheless, when the seedling picking frequency exceeds 100 seedlings per minute, the average substrate damage rate remains above 5%, accompanied by a noticeable drop in seedling picking success rate. This indicates that factors affecting the operation quality of the seedling picking mechanism at high speeds are not limited to the vibration of the planet carrier itself. Combined with test observations and the structural design of the seedling picking mechanism, the main causes of seedling picking failure and substrate damage during high-speed seedling extraction are summarized as follows: (1) Uneven growth of pot seedlings. Some pot seedlings feature loose substrate, which easily leads to picking failure or partial substrate shedding during seedling holding; (2) As the rotating speed of the picking arm rises, greater impact force is exerted on the substrate when the arm inserts into the plug tray, resulting in substrate damage. These influencing factors should be taken into account in subsequent design and optimization to further improve the working performance of the seedling picking mechanism.

Combined with experimental analysis, the optimized seedling picking mechanism can not only ensure the seedling picking success rate under high-speed operation conditions, but also reduce the substrate damage rate of potted seedlings, demonstrating an excellent operation performance. The results indicate that the EEMD-MA-based detection method proposed in this study is capable of vibration detection for the planetary wheel seedling picking mechanism. Through analysis on the vibration signals of the key components of the seedling picking mechanism, it is verified that the resonance phenomenon of key components is the dominant factor causing the degradation of seedling picking quality, which provides a theoretical basis for the structural optimization of the mechanism. Compared with the conventional research methods in existing literature that rely solely on modal simulation analysis, the proposed method integrates experimental measurement with finite element analysis, which effectively compensates for the theoretical errors of pure simulation analysis. This enables the structural optimization to be more consistent with actual operating conditions, significantly improves the reliability and practicability of vibration research, and provides a novel technical direction for the optimal design of seedling picking mechanisms of vegetable transplanters.

4 Conclusions

(1) An EEMD-MA method combining signal processing and finite element analysis was proposed. This method conducted multi-angle research and analysis on the planet carrier, the key component of the seedling picking mechanism, to obtain its vibration characteristics, which provides data support and theoretical basis for the optimal design of the planet carrier.

(2) The vibration signals of the planet carrier under high-speed operation were collected and processed by the wavelet soft threshold algorithm and EEMD method. Combined with the comprehensive index Y, the characteristic frequency of the planet carrier was determined to be 129.83 Hz. Meanwhile, modal analysis of the planet carrier was carried out via the finite element method, and its first-order natural frequency was found to be 128.65 Hz. The characteristic frequency extracted from the vibration signal is close to the first-order natural frequency obtained by finite element calculation, and both fall within the vicinity of the excitation characteristic frequency range. This condition is highly likely to trigger resonance and thus deteriorate the seedling picking operation quality.

(3) The sequential quadratic programming method was adopted for optimal design with the shell thicknesses of the planet carrier as design variables. After optimization, the thickness of the left shell is 9.7 mm and that of the right shell is 11.5 mm. Modal analysis was then performed on the optimized planet carrier. The results show that all orders of its natural frequencies deviate from the excitation frequency band, so resonance can be avoided effectively. In addition, vibration tests reveal that the vibration amplitude of the optimized planet carrier at the characteristic frequency is reduced by 61.36%, which greatly suppresses vibration intensity. Seedling picking tests under four operating frequencies demonstrate that the optimized mechanism achieves a certain increase in seedling picking success rate by 3.3%, 3.4%, 2.6%, and 1.8% respectively, while the substrate damage rate decreases by 13.53%, 11.88%, 9.15%, and 8.12% correspondingly. The optimized seedling picking mechanism can remarkably reduce substrate damage during seedling extraction, which verifies the effectiveness and practicability of the proposed method. Furthermore, this research method provides a novel idea and reference for the optimal design of various automatic seedling picking mechanisms.

Acknowledgements

This work was supported by the National Key Research and Development Program of China Project (Grant No. 2022YFD2001205), the Major Science and Technology Special Project of Henan Province (Grant No. 231100110200), the Henan Province Modern Agricultural Industry Technology System Robot Position Expert Project (Grant No. HARS-22-20-G1), and the Key Research and Development Special Project of Henan Province (Grant No. 241111114100).

[References]

[1] Yue R C, Hu J P, Liu Y J, Yao M J, Zhang T F, Shi J W. Design and working parameter optimization of pneumatic reciprocating seedling-picking device of automatic transplanter. Agriculture, 2022; 12(12): 1989.

[2] Xu Q C, Chen H Y, Liu C X, Zhu J T, Li S J, Ye M Q. Design of the filling device for citrus seedling pot based on turnover box. Int J Agric & Biol Eng, 2025; 18(3): 97–104.

[3] Li L H, Zhu C H, Liu B X, Li D H, Lyu Z, Xu L C, et al. Design and optimization of the seedling needle and push device for a mechanical transplanter of seedlings from bowl-type trays made of paddy straw. Int J Agric & Biol Eng, 2025; 18(6): 75–82.

[4] Yu Y X, Liu J K, Ye B L, Yu G H, Jin X J, Sun L, Tong J H. Design and experimental research on seedling pick-up mechanism of planetary gear train with combined non-circular gear transmission. Chinese Journal of Mechanical Engineering, 2019; 32(1): 49.

[5] Hu S Y, Hu M J, Zhang W Y. Design and experiment of flexible clamping device for pepper plug seedlings. Advances in Mechanical Engineering, 2022; 14(6): 16878132221107254.

[6] Wang L, Lin Z W, Zhou Z H, Yu G H, Yang Z Y, Yu X F, et al. Design and experiment of a vegetable plug seedling planting mechanism combining non-circular gear system and multi-link. Int J Agric & Biol Eng, 2025; 18(3): 124–134.

[7] Du F J, Yu G H, Liu J G, Qi P, Ao M, Wang L. A novel tooth profile for low-tooth-count gears: design methodology and application in noncircular gear transmission mechanism. International Journal of Precision Engineering and Manufacturing, 2026: 1–19. DOI: 10.1007/s12541-026-01480-1.

[8] Khadatkar A, Pandirwar P, Paradkar V. Design, development and application of a compact robotic transplanter with automatic seedling picking mechanism for plug-type seedlings. Scientific Reports, 2023; 13(1): 1883.

[9] Zhou M L, Sun L, Du X Q, Zhao Y, Xin L. Optimal design and experiment of rice pot seedling transplanting mechanism with planetary Bezier gears. Transactions of the ASABE, 2014; 57(6): 1537–1548.

[10] Ye B L, Wang X W, Tang T, Zeng G J, Zheng Y. Design and tests of a planetary non-circular gear train transplanting mechanism for flower plug seedlings. Mechanical Sciences, 2025; 16(2): 303–316.

[11] Yin J J, Wang Z L, Zhou M L, Wu L N, Zhang Y. Optimized design and experiment of the three-arm transplanting mechanism for rice potted seedlings. Int J Agric & Biol Eng, 2021; 14(5): 56–62.

[12] Liu J P, Yu G H, Tong Z P, Hua Y. Design and experimental study of a planetary gearing mechanism based on twice unequal amplitude transmission ratio. Int J Agric & Biol Eng, 2022; 15(1): 155–163.

[13] Hu S Y, Hu M J, Yan W, Zhang W Y. Design and experiment of an integrated automatic transplanting mechanism for picking and planting pepper hole tray seedlings. Agriculture, 2022; 12(4): 557.

[14] Su Q, Li X Y, Zeng F D, Wang J Y, Zhang Y Z, Bai H B, Wu L, Wang J. Vibration characteristics test and analysis of hanging cup transplanter. INMATEH-Agricultural Engineering, 2022; 66(1). DOI: 10.35633/inmateh-66-28.

[15] Chowdhury M, Reza M N, Kabir M S N, Kiraga S, Kin S J, Choi L S, et al. Vibration assessment of a 12-kw self-propelled riding-type automatic onion transplanter for transplanting performance and operator comfort. Applied Sciences, 2023; 13(3): 1927.

[16] Zhu D Q, Gao K J, Xue K, Zhang S, Liao J, Wang T J, et al. Vibration analysis and parameter optimization of seedling pushing device of transplanting mechanism with planetary elliptic gears. Journal of the Chinese Institute of Engineers, 2023; 46(2): 154–162.

[17] Ji J T, Chen K K, Jin X, Wang Z Y, Dai B Q, Fan J Y, et al. High-efficiency modal analysis and deformation prediction of rice transplanter based on effective independent method. Computers and Electronics in Agriculture, 2020; 168: 105126.

[18] Chen S R, Zhao Y P, Tang Z, Lu S N. Modal vibration response of rice combine harvester frame under multi-source excitation. Biosystems Engineering, 2020; 194: 177–195.

[19] Jin X, Zhang B, Suo H B, Lin C, Ji J T, Xie X L. Design and mechanical analysis of a cam-linked planetary gear system seedling picking

mechanism. Agriculture, 2023; 13(4): 810.

[20] Liu M P, Sun X H, Wang Q N, Deng S H. Short-term load forecasting using EMD with feature selection and TCN-based deep learning model. Energies, 2022; 15(19): 7170.

[21] Guo R X, Wang Y, Zhang H C, Zhang G L. Remaining useful life prediction for rolling bearings using EMD-RISI-LSTM. IEEE Transactions on Instrumentation and Measurement, 2021; 70: 1–12.

[22] Cao Y, Hou X L, Chen N. Short-term forecast of OD passenger flow based on ensemble empirical mode decomposition. Sustainability, 2022; 14(14): 8562.

[23] Li Y, Zhou J W, Li H G, Meng G, Bian J. A fast and adaptive empirical mode decomposition method and its application in rolling bearing fault diagnosis. IEEE Sensors Journal, 2022; 23(1): 567–576.

[24] Pan H Y, Zheng J D, Yang Y, Cheng J S. Nonlinear sparse mode decomposition and its application in planetary gearbox fault diagnosis. Mechanism and Machine Theory, 2021; 155: 104082.

[25] Liu Z L, Li M G, Zhu Z F, Xiao L H, Nie C H, Tang Z C. Health state identification method of nuclear power main circulating pump based on EEMD and OQGA-SVM. Electronics, 2023; 12(2): 410.

[26] Zhou X, Zhao H, Jiang T. Adaptive analysis of optical fringe patterns using ensemble empirical mode decomposition algorithm. Optics Letters, 2009; 34(13): 2033–2035.

[27] Guo Y Y, Si J C, Wang Y L, Hanif F, Li S, Wu M W, et al. Ensemble-Empirical-Mode-Decomposition (EEMD) on SWH prediction: The effect of decomposed IMFs, continuous prediction duration, and data-driven models. Ocean Engineering, 2025; 324: 120755.

[28] Zadeh L. Probability measures of fuzzy events. Journal of Mathematical Analysis and Applications, 1968; 23(2): 421–427.

[29] Tran M Q, Elsis M, Liu M K. Effective feature selection with fuzzy entropy and similarity classifier for chatter vibration diagnosis. Measurement, 2021; 184: 109962.

[30] Xin G, Ying L. Multi-attribute decision-making based on comprehensive hesitant fuzzy entropy. Expert Systems with Applications, 2024; 237: 121459.

[31] Zhang Y F, Li Y H, Kong L F, Niu Q B, Bai Y. Improved DBSCAN spindle bearing condition monitoring method based on kurtosis and sample entropy. Machines, 2022; 10(5): 363.

[32] Pang J, Lin Y, Wang S S, Du Z, Xie L L, Chen X Q. Vibration analysis and structure optimization of grain cleaning screen based on VMD. Transactions of the CSAE, 2023; 39(12): 1–9. (in Chinese)